Computational Study Of Dense Granular Flows In Stirred Reactors

Lokman Bennani[1], Hervé Neau[1], Cyril Baudry[2], Jérôme Laviéville[2], Pascal Fede[1] and Olivier Simonin[1]

[1] *Institut de Mécanique des Fluides de Toulouse (IMFT), Université de Toulouse, CNRS, INPT, UPS, FR-31400 Toulouse FRANCE*

[2] *EDF - R & D, Département MFEE, 6 quai Watier, FR-78401 Chatou, France*

Abstract

In chemical engineering applications, reactors featuring rotating parts are common practice. As these rotating parts are present in order to enhance chemical reactions, it is essential to take them into account when performing predictive numerical simulations. This aspect can be particularly challenging, even more so when complex industrial geometries are to be treated. In this communication the rotating mesh numerical methodology of NEPTUNE_CFD V3.0 (an Eulerian n-fluid multiphase flow CFD code) is presented. The method is based on splitting the domain into static and rotating parts. The information between rotating and static parts is passed thanks to a non-conformal mesh matching technique. The methodology is first validated, both numerically and experimentally using the classical rotating drum case. The high degree of compaction of the flow is taken into account thanks to a frictional stress tensor. The method is then pushed further and used to investigate the hydrodynamics of dry granular beds in stirred vessels. The results show that the rotating mesh method can effectively treat such configurations, hence offering interesting insight concerning the dynamics of the flow.

Keywords: Granular flow, Numerical simulation, Rotating mesh, Rotating drum, Frictional stress

1. Introduction

Flow of granular materials in rotating geometries is a frequent aspect of chemical engineering applications[4, 16]. The rotating motion is often used so as to enhance the chemical process. Experimental investigation of large scale chemical reactors involving such a motion is often complicated. Hence there is a need for efficient numerical simulation strategies which are able to capture the flow of granular materials in rotating geometries.

A possible numerical approach is the Discrete Element Method (DEM). In effect, this method has been used to investigate flat bladed stirrers or rotating drums [1, 19, 13]. However, DEM is limited by the number of particles that have to be tracked [6].

Another method is to solve the flow equations in an Eulerian framework, which is the one adopted in this work. This approach doesn't have the previously discussed drawback and is hence more suited for the simulation of large scale reactors [18]. However, taking rotating parts into account is more complicated. Indeed, if the geometry of interest features rotational symmetries a possible solution is to solve the governing flow equations in a rotating frame of reference or by using sliding wall boundary conditions (well adapted to rotating drums for instance), as done in references [8, 14]. However, in most problems such symmetries are not present. This can be due, for example, to the presence of chimneys or extraction pipes. In these cases, a more elaborate numerical strategy is needed.

In this communication, a rotating mesh method for simulating unsteady granular flows in complex large scale geometries is presented. It is a first step towards solving the aforementionned problems. The main idea is to split the domain into static and rotating parts and to use a non-conformal mesh matching technique to connect the domains [7].

Firstly, the physical modelling and rotating mesh method are presented. Secondly, the validation of the method is addressed using the classic rotating drum case. Finally, the method is pushed into the industrial realm by demonstrating its applicability to a prototype of a horizontally stirred reactor.

2. Physical Model

The physical modelling is largely based on a particulate Eulerian approach. It is derived from a joint fluid-particle PDF equation allowing to obtain the transport equations for the mass, momentum and fluctuating kinetic energy of particle phases [15].

In addition, the flows under consideration in this study present a high degree of compaction. This means that frictional interaction between solid particles is an important aspect and has to be taken into account. This is done through the introduction of a frictional part in the stress tensor in the momentum equation.

The particle phase stress tensor $\underline{\underline{\Sigma}}_p$ is modeled as the sum of a kinetic-collisional part derived in the frame of the kinetic theory of rapid granular flow modified by the drag force [5], $\underline{\underline{\Sigma}}_p^g$ and a frictional part, $\underline{\underline{\Sigma}}_p^f$. Hence it is given by $\underline{\underline{\Sigma}}_p = \underline{\underline{\Sigma}}_p^g + \underline{\underline{\Sigma}}_p^f$.

The collisional/kinetic part of the particle phase stress tensor is written using a viscosity assumption:

$$\Sigma_{p,ij}^g = \left[P_p - \lambda_p \frac{\partial U_{p,k}}{\partial x_k} \right] \delta_{ij} - \mu_p S_{p,ij} \,, \tag{1}$$

where P_p is the granular pressure, λ_p the bulk granular viscosity and μ_p the kinetic-collisional viscosity. Moreover, $\underline{\underline{S}}_p$ is defined in the following way:

$$S_{p,ij} = \frac{\partial U_{p,i}}{\partial x_j} + \frac{\partial U_{p,j}}{\partial x_i} - \frac{2}{3} \frac{\partial U_{p,k}}{\partial x_k} \delta_{ij} \,. \tag{2}$$

Concerning the frictional part of the stress tensor, the approach proposed by [17] is retained. It is based on rheological laws used in soil mechanics which assume that, in the high compaction regime, the granular material follows a rigid-plastic behaviour. In this context, Srivastava and Sundaresan propose the following model for the frictional stress:

$$\underline{\underline{\Sigma}}_p^f = p_c \mathbb{I} - \sqrt{2} \sin(\phi) p_c \frac{\underline{\underline{S}}_p}{\sqrt{\underline{\underline{S}}_p : \underline{\underline{S}}_p + \frac{8 q_p^2}{3 d_p^2}}} \,, \tag{3}$$

where d_p is the particle diameter, ϕ is the angle of internal friction, q_p^2 is the particle kinetic agitation and $8q_p^2/3d_p^2$ is an estimate for strain rate fluctuations. p_c is the critical state pressure defined by:

$$p_c(\alpha_p) = \begin{cases} F\frac{(\alpha_p-\alpha_{p,min})^r}{(\alpha_{p,max}-\alpha_p)^s} & \text{if } \alpha_p > \alpha_{p,min} \\ 0 & \text{if } \alpha_p \leq \alpha_{p,min} \end{cases} \quad (4)$$

where F, r, s are constants. The different parameters used here to define the frictional model are summed up in table 1. It should be noted that the values were taken as given by [17]. They were not optimized for the cases studied in this work.

$\alpha_{p,min}$	$\alpha_{p,max}$	$F(Pa)$	r	s
0.5	0.64	0.05	2	5

Table 1: Frictional model parameters.

3. The Rotating Mesh Method

The numerical simulations presented in this communication have been carried out using an Eulerian n-fluid modeling approach for gas-solid turbulent polydisperse flows developed and implemented by IMFT (Institut de Mécanique des Fluides de Toulouse) in the NEPTUNE_CFD 3.0 version. NEPTUNE_CFD is a multiphase flow software developed in the framework of the NEPTUNE project, financially supported by CEA (Commissariat à l'Energie Atomique), EDF (Electricité de France), IRSN (Institut de Radioprotection et de Sûreté Nucléaire) and AREVA-NP. The numerical solver has been developed for High Performance Computing [12, 11].

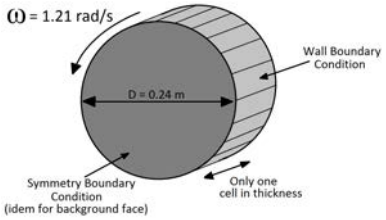

(a) Sketch of the drum

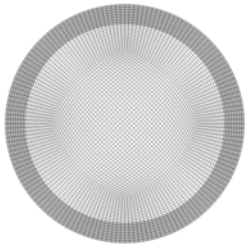

(b) Mesh of the rotating drum

Figure 1: Mesh of the rotating drum.

The rotating mesh method considered here operates by taking as inputs several meshes, some of them will be fixed, others will be rotating. The equations of motion are solved in each mesh in the absolute frame of reference. For the rotating mesh, the governing equations must be formulated so as to take into account its motion. To do so, an ALE-like (Arbitrary Lagrangian-Eulerian) approach is used [3].

In order to assess the method a first purely numerical validation is performed. The case consists in a drum which is rotated at $\omega = 1.21 rad.s^{-1}$ and initially uniformly filled with gas and particles with volume fractions respectively $\alpha_g = 0.56$ and $\alpha_p = 0.44$ (see Figure 1(a)). The case is simulated with the rotating mesh method and with a conventional sliding wall approach. The results of these two computations are compared. Moreover, as this case is purely numerical, gravity is not present. In this case, the variables are always extracted along the x axis, from the center of the drum to its boundary.

The mesh (Figure 1(b)) is composed of 1280 cells in the crown and 3840 cells in the fixed area, making a total of 5120 cells. Tests performed with a more refined mesh (32000 cells) showed that the considered mesh is sufficiently refined to yield mesh independant results.

The density of the gas is set to $\rho_g = 1.2\,\mathrm{kg.m^{-3}}$ and its viscosity to $\mu_g = 1.85\,10^{-5} Pa.s$. Table 2 gives the physical parameters of particle phase (glass beads).

particle density ρ_p	diameter d_p
$2500\mathrm{kg.m^{-3}}$	$3\,.10^{-3}\mathrm{m}$
Elastic coefficient	Internal friction angle
0.9	25°

Table 2: Particle phase physical properties.

As the flow exhibits a rotational symmetry, the solid volume fractions are plotted along the radial direction. They are shown in Figure 2. As can be seen, a very good agreement between both methods is achieved.

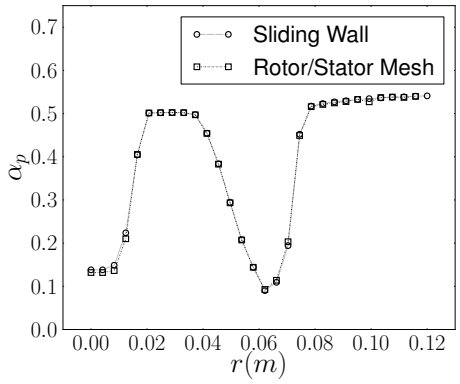

Figure 2: Comparison of solid volume fractions at $t = 30$s.

Coherently with the previously observed trend, tangential velocities match almost perfectly as can be seen in Figure 3.

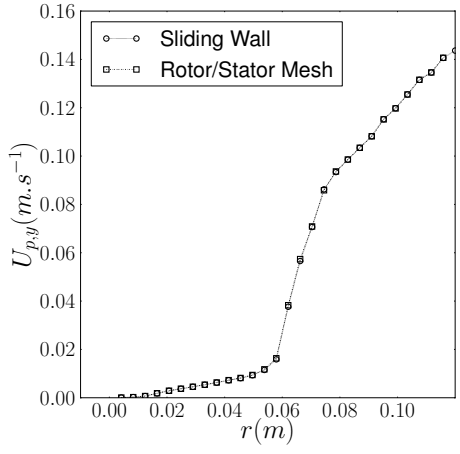

Figure 3: Comparison of the tangential velocities at $t = 30$s.

The above results show that the rotating mesh method is fully able of correclty reproducing the numerical results obtained with a conventional sliding wall approach. However, the rotating mesh method is more computationally expensive due to the non-conformal mesh matching which is required at each time iteration. Table 3 provides an idea of this additional cost.

	Time
Rotor/Stator	$730s$
Sliding Wall	$590s$

Table 3: CPU times to simulate $40s$ of physical time (on two cores).

It should also be noted that the rotation imposes a restriction on the time step. Indeed, so as to remain consistent with respect to the flow physics, the curvilinear distance traveled by the rotating mesh at the joining interface during a given time step should not exceed that of a mesh cell. In other words: $\omega R_j \Delta t \leq \Delta s_j$, where R_j is the joining radius between rotor and stator and Δs_j is the cell size in the tangential direction.

4. The Rotating Drum Test Case

The experimental case used for validation is the second monodisperse case of [2] (which they denote MD2). With respect to the simulations of section 3, the setting differs only by the presence of gravity and by the initial filling. In particular, the frictional viscosity parameters and the particle physical properties are those of tables 1 and 2. The drum is filled to 35% in volume with solid particles, in accordance with the experimental setup. The case is illustrated by Figure 4, where the data extraction axes are also shown.

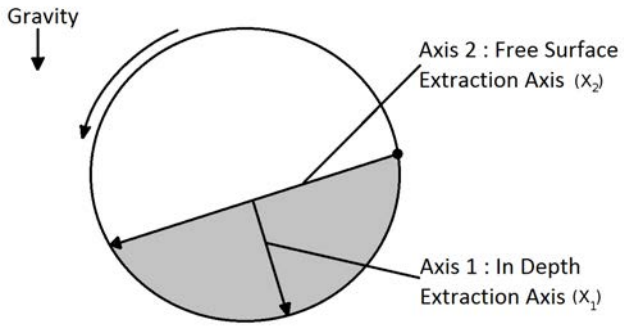

Figure 4: Location of the data extraction axes.

Note that Alizadeh et al. use non-dimensional variables for the velocity profile extracted along the free surface. This is performed by using the following theoretical velocity profile [9, 10]:

$$\frac{U_{fs}}{U_{max}} = 1 - \left(\frac{x_2}{L}\right)^2 \tag{5}$$

where $U_{max} = \frac{\omega L^2}{\delta_0}$, L the half-length of the free surface. δ_0 is the distance from the free surface to the active-passive layer transition, that is to say the distance from the free surface to the point where the velocity changes direction.

U_{max} is used in [2] to nondimensionalize the velocities on the free surface and hence will also be used here (with values taken from [2]: $L = 0.115\text{m}$, $\delta_0 = 0.033\text{m}$).

Figure 5 shows the velocity profile perpendicular to the extraction axis (axis 1 in Figure 4). This velocity profile is characteristic of rotating drums in rolling mode [4]. Starting at the wall, the velocity profile first presents a region of almost rigid body type motion, hence correctly capturing the main feature of the so-called passive layer. As the depth is lowered the velocity decreases until it changes direction, marking the passage from passive to active layer. This feature of the flow is well captured, as can be seen in Figure 5. Moreover, good quantitative agreement is achieved between the numerical prediction and experiment. However, note that the maximum speed, which is reached at the free surface, is underestimated.

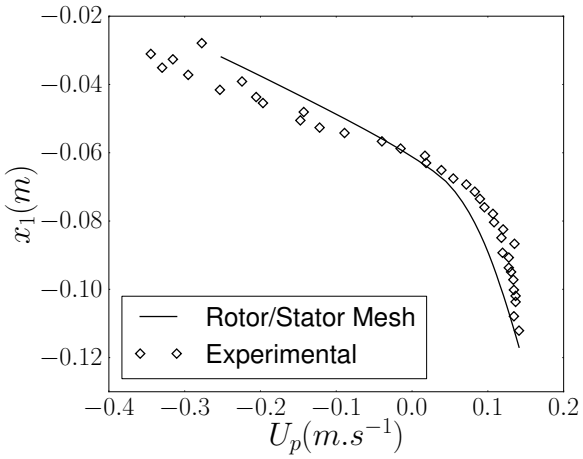

Figure 5: Comparison of velocity profiles in the depth of the particle bed.

The second velocity profile of interest is that extracted at the free surface. It is shown by Figure 6. This profile describes another fundamental aspect of this flow regime which is the rolling down motion. Indeed, the velocity along the freestream starts at almost zero magnitude and increases approximately until the mid point of the free surface. At this point the velocity along the free stream decreases until the end of the free surface, where the particles are then taken back into the passive layer. This aspect of the flow is qualitatively well predicted. Nevertheless, the magnitude is underestimated.

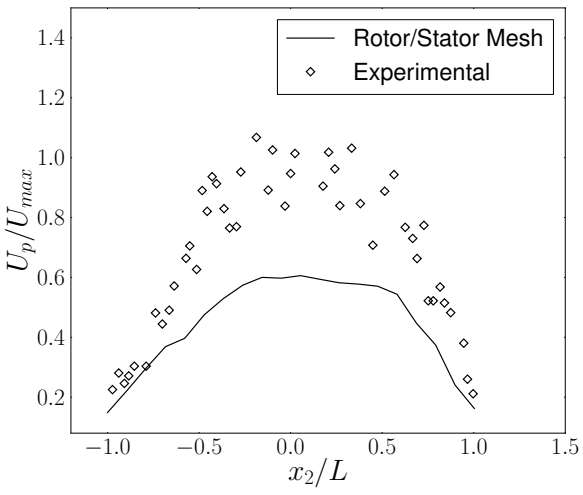

Figure 6: Comparison of velocity profiles at the free surface of the particle bed.

Another interesting point is the tilt angle taken by the particle bed due to the drum's rotation. Figure 7 shows the solid volume fraction field. The white line is the separation between active and passive layers. The tilt and separation between active and passive

layers are qualitatively well captured. However, the tilt angle obtained by simulation is of 15° while the one present in Alizadeh et al.'s experiments is of 27°. The fact that the velocity at the free surface is underestimated is consistent with this observation.

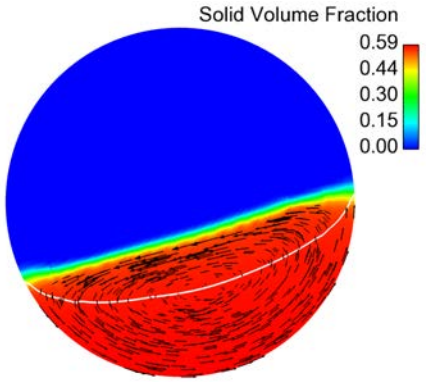

Figure 7: Tilting of the solid particle bed: the black arrows represent the particle velocity field while the white line delimits the active and passive layers.

The tilting comes from the addition of the frictional stress component. Indeed it enables momentum to be transmitted from the rotating wall through the particle bed thanks to the additional frictional viscosity. However, on a more quantitative side, the predicted angle is noticeably different from that observed experimentally. The simulation was also performed using the sliding wall approach and predicted the same tilt angle. Hence, considering both numerical methods predict the same tilt angle, improvements on this point are to be sought more in the frictional stress model.

5. Towards Large Scale Industrial Applications: Prototype of a Horitzontally Stirred Reactor

In this final section, the applicability of the rotating mesh method to full scale industrial problems is demonstrated. Indeed, it is for these kinds of complex applications that the method proves to be the most usefull. In this section, the hydrodynamics of a gas-particles flow inside a numerical prototype of a horizontally stirred reactor is simulated. As can be seen in Figure 8, the numerical prototype has a chimney. This means that the use of methods based on rotational symmetries would not have been possible.

5.1. Geometry and Mesh

The geometry of the reactor is strongly inspired from the illustrations that can be found in [16]. It is composed of a horizontal stirrer and a chimney, as can be seen in Figure 8(a). As stated in reference [16], the horizontal vessel is usually $10-15\,\mathrm{m}$ long and $1.5-4\,\mathrm{m}$ in diameter. Therefore, in the case of our numerical prototype, the vessel is $11\,\mathrm{m}$ long and $4\,\mathrm{m}$ in diameter. Also, the chimney is $6\,\mathrm{m}$ high.

The rotating part is the axial stirrer contained within the horizontal vessel whereas the static (stator) part is the rest of the vessel and the chimney (see Figure 8(b)). It should be noted that this is not a reproduction of an actual reactor. It is a numerical prototype designed only to demonstrate the applicability of the method to industrial scale problems.

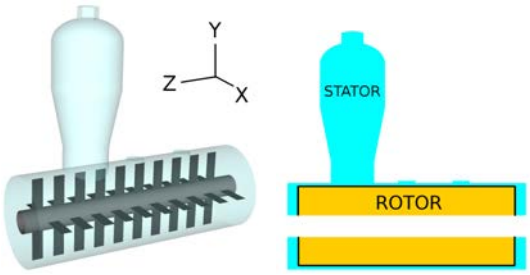

(a) Global view of the reactor and stirrer. (b) Rotating and static parts.

Figure 8: View of the geometry.

The mesh was composed of 1.3 million hexahedral elements. The rotating part was meshed with $600\,000$ elements and the static part with $700\,000$ elements. The resulting mesh is shown in Figure 9.

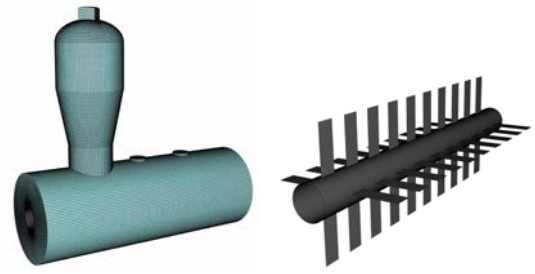

(a) Global view of the mesh. (b) The axial stirrer.

Figure 9: View of the mesh.

5.2. Results and Discussion

In this case, the reactor is filled with 25 tonnes of particles (located in the horizontal vessel). Their density is $\rho_p = 500\,\mathrm{kg.m^{-3}}$ and they have a diameter of $d_p = 0.5\,\mathrm{mm}$. This is equivalent to more than 10^{10} particles in the reactor.

It should be noted that for this case, the flow of the gas phase can no longer be assumed laminar. Hence, a $k-\epsilon$ model which includes additional terms accounting for the influence of the particles on the fluid turbulence is used.

The hydrodynamics may first be investigated by looking at the solid volume fraction. Figure 10 shows solid volume fractions at the skin of the reactor. A kind of wavy structure is observed which is due to the blades passing and projecting particles towards the boundaries. Moreover, the peaks of the waves are shifted coherently with the blades that are passing by.

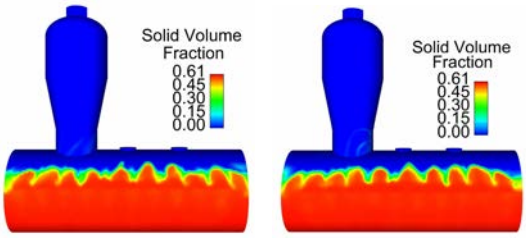

(a) First pass. (b) Second pass.

Figure 10: Solid volume fraction at the boundaries after two consecutive blade passes.

Figure 11 shows solid volume fractions in an YZ cut. Here again, structures are formed by the blade motion which sends the particles upwards.

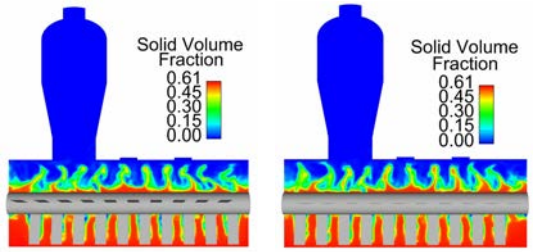

(a) First pass. (b) Second pass.

Figure 11: YZ cut: solid volume fraction after two consecutive blade passes.

It is also of interest to look at the particle velocity fields. Let's first consider a cut in the YZ plane, as shown in Figure 12(a). The cut is done just after a set of blades has passed through the plane. In the upper half, the velocity vectors show a complex pattern. Where the blade has just passed the particles are pushed upwards. On the other hand, the particles in the most upper part of the vessel are moving back down, creating the kind of circular pattern which is observed.

Secondly, let's consider a cut in the XY plane (Figure 12(b)). The cut is done at the same time as the one in the YZ plane. However, note that the cut is performed so as to intersect with a blade that is almost at 0°. Here also, complex patterns can be observed, with particles being pushed upwards, others falling back down and the bulk of the bed being stirred at the bottom.

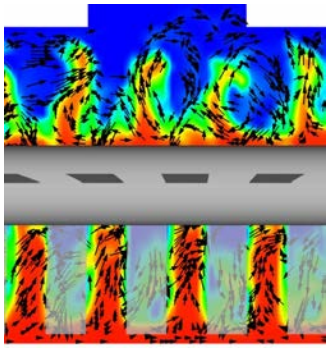

(a) Cut in the YZ plane.

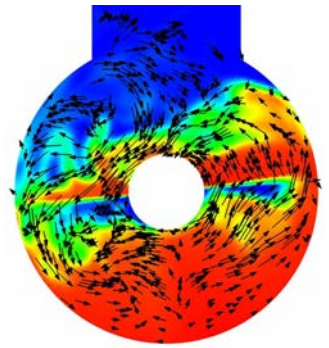

(b) Cut in the XY plane (beneath the chimney).

Figure 12: Solid volume fraction and particle velocity vector fields in an YZ and XY cut (see Figure 8(a) for axes).

Finally, the dispersion of a passive scalar can also give usefull information. Here, the passive scalar is transported by the gas phase. As shown in Figure 13, the passive scalar, originally located beneath the chimney, is gradually dispersed inside the reactor. This enables to get an idea of the mixing properties of the reactor in a given set of operating conditions.

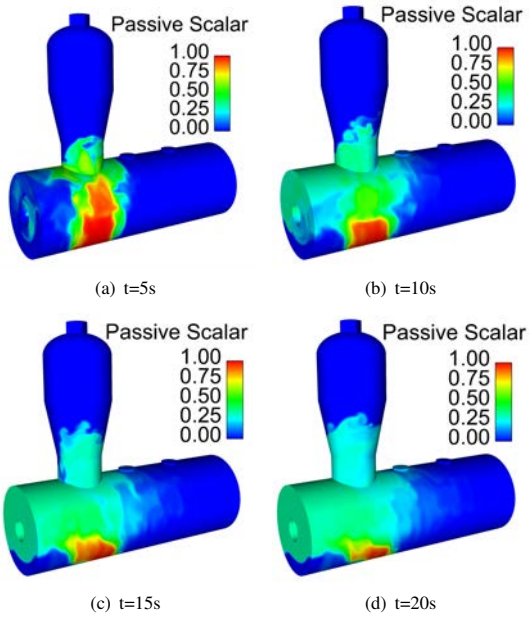

(a) t=5s (b) t=10s

(c) t=15s (d) t=20s

Figure 13: Transport of a passive scalar by the gas phase at four consecutive times.

6. Conclusions and Perspectives

In this communication a rotating mesh method for simulating dense gas-particle flows in rotating geometries has been presented. Within the framework of an Eulerian n-fluid modeling approach, this method enables to treat problems featuring complex geometries.

First, the modelling and numerical method was presented. The method was numerically validated by comparing its results with a conventional sliding wall approach.

Secondly, an experimental setup of a rotating drum was simulated. The experimental velocity profiles were compared to the numerical predictions of the rotating mesh method. The numerical results were in good agreement with the experimental data and the rolling regime flow pattern was correctly captured. The comparisons with experimental data were performed for a given set of model parameters taken from the literature. This set of parameters leads to a correct prediction of the in-depth velocity profile. However, improved modelling is required in order to better capture the free surface velocity and the tilt angle. It is interesting to note that in the frictional model, a term in q_p^2 is present in the denominator. This term represents fluctuations in strain rate [17]. If it is of the same order of magnitude as $\underline{\underline{S}}_p : \underline{\underline{S}}_p$ at the bottom of the drum then it will have a strong impact on the frictional stress tensor. Investigations on this point are part of current work.

Finally, the applicability of the method to industrial size complex problems was demonstrated. Indeed, the method was used to investigate the hydrodynamics of the gas-particle flow inside a fictious prototype of a horizontally stirred reactor. This enabled to identify several flow patterns and hence opens the doors to interesting investigations of gas-particle flows in complex geometries.

Overall, the rotating mesh method therefore presents an interesting perspective for the Eulerian simulation of dense granular

flows in rotating geometries. The gain in using this method is that it allows to simulate complex problems of industrial size. For example, a configuration of interest is the simulation of a full scale chemical reactor featuring chimneys and other complex parts, and including the modelling of chemical reactions. This aspect is part of ongoing work.

Acknowledgments

This work was granted access to the HPC resources of CALMIP supercomputing center under the allocation 2015-0111. This work was performed using HPC resources from GENCI-CINES (Grant 2015-c20152b6012).

References

[1] E. Alizadeh, F. Bertrand, and J. Chaouki. Comparison of DEM results and Lagrangian experimental data for the flow and mixing of granules in a rotating drum. *AIChE Journal*, 60(1):60–75, 2014.

[2] E. Alizadeh, O. Dubé, F. Bertrand, and J. Chaouki. Characterization of mixing and size segregation in a rotating drum by a particle tracking method. *AIChE Journal*, 59(6):1894–1905, 2013.

[3] B. Audebert. Code_saturne, mise en place et validation de la fonctionalité couplage rotor / stator pour la modélisation des pompes. Technical Report H-I85-2009-00430-FR, EDF, 2009.

[4] A. A. Boateng. *Rotary Kilns: Transport Phenomena and Transport Processes*. Butterworth-Heinemann, 2011.

[5] A. Boëlle, G. Balzer, and O. Simonin. Second-order prediction of the particle-phase stress tensor of inelastic spheres in simple shear dense suspensions. In *Gas-Particle Flows*, volume 228, pages 9 – 18. ASME FED, 1995.

[6] J. Capecelatro and O. Desjardins. An euler–lagrange strategy for simulating particle-laden flows. *Journal of Computational Physics*, 238:1–31, 2013.

[7] EDF. *Code Saturne 3.3.0 Theory Guide*. EDF R & D, http://code-saturne.org/cms/sites/default/files/docs/3.3/theory.pdf, May 2014.

[8] A. N. Huang, W. C. Kao, and H. P. Kuo. Numerical studies of particle segregation in a rotating drum based on eulerian continuum approach. *Advanced Powder Technology*, 24(1):364–372, 2013.

[9] D. V. Khakhar, J. J. McCarthy, and J. M. Ottino. Radial segregation of granular mixtures in rotating cylinders. *Physics of Fluids (1994-present)*, 9(12):3600–3614, 1997.

[10] D. V. Khakhar, J. J. McCarthy, T. Shinbrot, and J. M. Ottino. Transverse flow and mixing of granular materials in a rotating cylinder. *Physics of Fluids (1994-present)*, 9(1):31–43, 1997.

[11] H. Neau, P. Fede, J. Laviéville, and O. Simonin. High performance computing (HPC) for the fluidization of particle-laden reactive flows. In *The 14th International Conference on Fluidization - From Fundamentals to Products*, ECI Symposium Series, 2013.

[12] H. Neau, J. Laviéville, and O. Simonin. Neptune CFD high parallel computing performances for particle-laden reactive flows. In *7th International Conference on Multiphase Flow, ICMF 2010, Tampa, FL, May 30 - June 4*, 2010.

[13] B. Remy, J. Khinast, and B. Glasser. Discrete element simulation of free flowing grains in a four-bladed mixer. *AIChE Journal*, 55(8):2035–2048, 2009.

[14] D. A. Santos, I. J. Petri, C. R. Duarte, and M. A. S. Barrozo. Experimental and CFD study of the hydrodynamic behavior in a rotating drum. *Powder Technology*, 250:52–62, 2013.

[15] O. Simonin. Combustion and turbulence in two-phase flows. In *Lecture Series 1996-02*. Von Karman Institute for Fluid Dynamics, 1996.

[16] J. Soares and T. McKenna. *Polyolefin Reaction Engineering*. John Wiley & Sons, 2013.

[17] A. Srivastava and S. Sundaresan. Analysis of a frictional–kinetic model for gas–particle flow. *Powder technology*, 129(1):72–85, 2003.

[18] Z. Zeren, H. Neau, P. Fede, O. Simonin, B. Descales, and W. Stephens. Numerical study of solid particle axial mixing in a fixed cylindrical drum with rotating paddles. In *AIChE Annual Meeting*, 2012.

[19] Y C Zhou, A B Yu, and J Bridgwater. Segregation of binary mixture of particles in a bladed mixer. *Journal of Chemical Technology and Biotechnology*, 78(2-3):187–193, 2003.